Arch. Metall. Mater. **67** (2022), 4, 1267-1276

DOI: https://doi.org/10.24425/amm.2022.141051

QI AN[1,2], DONGTING WU[1*], PENG LIU[3], YONG ZOU[4*]

LASER WELDING OF TA15 TITANIUM ALLOY AND INCONEL 718 DISSIMILAR METALS

This paper studied the effect of laser welding technology on dissimilar metal welding joints of TA15 titanium alloy and Inconel 718 nickel-based alloy. The research results indicate that the laser welding of TA15 titanium alloy and Inconel 718 nickel-based alloy directly was difficult to form well, which due to the intermetallic compounds caused the joint brittle. When the pure Cu foil was used as the filling layer, the quality of the welding joints can be improved effectively. The experimental results also indicate that there were brittle intermetallic-compounds in the laser welding seam, and the laser power had an important influence on the performance and mechanical properties of the dissimilar metal joint. The maximum average tensile strength of the welding joint of 2300 W was increased to 252.32 MPa. Scanning electron microscope(SEM) results show that the fracture morphology was river pattern, a typical morphological of cleavage fracture, and the mode was brittle fracture.

Keywords: TA15 titanium alloy; Inconel 718 nickel-based alloy; laser welding; microstructure; tensile strength and fracture characteristic

1. Introduction

Titanium alloys have been widely applied in medical and aerospace fields because of their high strength-to-weight ratio, excellent biocompatibility, superior erosion resistance and creep resistance [1-3]. Among them, the TA15 alloy has a high Al equivalent, belonging to Ti-Al-Zr-Mo-V series [4,5]. Inconel 718 nickel-based alloy is a kind of precipitation-hardening super alloy, which is also wildly used in aerospace because of its superior mechanical properties, outstanding corrosion resistance and high temperature oxidation resistance, high strength and thermal stability in the high temperature environment of 700~900°C [6,7]. The combination of the titanium alloy and the nickel-based alloy forming as the bimetallic structure can not only reduce the structural weight, but also fully uses their individual properties in the field of aerospace [8-10]. However, it is still challenging to achieve high-performance joints between these two dissimilar metals. On the one hand, there is a large difference in the coefficient of thermal expansion, which would easily induce large residual stress during welding joint. On the other hand, the brittle Ti-Ni intermetallic compounds can be formed readily inside the joint [11-13]. To overcome these issues, the addition of interlayer has been highlighted to effectively suppress the formation of these intermetallic compounds [14,15]. Furthermore, the utilization of laser welding technique is beneficial for reducing the thermal deformation and improving welding joints completeness due to the high laser beam energy and narrow heat affected zone [16]. Therefore, it is appropriate to welding joints the dissimilar metals.

To date, a number of researches have performed to investigate the laser welding joints process between the nickel alloy and the titanium alloy dissimilar metals [17]. Shang et al. [18] used the laser additive manufacturing (LAM) technology to fabricate the Ti-Ni bimetallic structures, and found that adding Nb/Cu interlayers could prohibit the formation of brittle phases. Accordingly, the tensile strength of the joint was increased to 283 MPa. Shojaei Zoeram et al. [19] studied the mechanical properties and fracture behavior of the laser welding joints joint between the NiTi shape memory alloy and Ti6Al4V alloy with Cu foil as the middle layer. They pointed out that the tensile strength increased with the increase of the Cu layer thickness and the tensile strength reached 300 MPa with a 75 μm thickness Cu foil. Shamini Janasekaran et al. [20] investigated the mechanical properties of T-type welding joint between the Ti6Al4V titanium alloy and the

[1] SHANDONG UNIVERSITY, KEY LABORATORY OF LIQUID-SOLID STRUCTURAL EVOLUTION AND PROCESSING OF MATERIALS, MINISTRY OF EDUCATION, JINAN, 250061, CHINA
[2] SHANDONG UNIVERSITY, SCHOOL OF MATERIALS SCIENCE AND ENGINEERING, JINAN, 250061, CHINA
[3] SHANDONG JIANZHU UNIVERSITY, SCHOOL OF MATERIALS SCIENCE AND ENGINEERING, JINAN, 250101, CHINA
[4] SHANDONG UNIVERSITY, JINAN SHANDONG ENGINEERING & TECHNOLOGY RESEARCH CENTER FOR MODERN WELDING, 250061, CHINA

* Corresponding authors: yzou@sdu.edu.cn, wudongting@sdu.edu.cn

Inconel 600 nickel base alloy, and the results indicated that the maximum fracture force was about 150 N when the laser power of welding joints was 250 W, the laser scan speed was 40 mm/s and 50% overlap rate. However, there are still some challenges for welding of TA15 titanium alloy and Inconel 718 dissimilar metal. On the one hand, the composition of Inconel 718 Alloy is more complex, so the types of brittle intermetallic compounds in weld zone increase. On the other hand, there are few studies on butt welds of TA15 titanium alloy and Inconel 718 dissimilar metal with Cu addition layer. Therefore, dissimilar metals of TA15 titanium alloy and Inconel 718 nickel base alloy were joined by laser welding joints in this paper. The effect of Cu foil as the filler layer on the mechanical properties of welding joints was studied by comprehensively analyzing the microstructure and fracture morphology of the joints.

2. Experiment procedure

2.1. Materials and Welding Method

The TA15 sheets and Inconel 718 sheets with a thickness of 2 mm, a length of 120 mm, and a width of 100 mm, were used as the base metals while the pure Cu foil with the size of 2 mm width and 1 mm thickness was selected as the interlayer. The chemical compositions were listed in TABLE 1.

All these sheets were ultrasonically cleaned in acetone for 5 minutes before welding. Afterwards, the base materials were clamped properly and a fiber laser (YLS-10000, IPG) was employed for welding joints. The welding speed was kept 25 mm/s, the laser spot diameter was 0.3 mm and the defocusing amount was 0 mm. Furthermore, different laser power of 2100 W, 2300 W, 2500 W and 2700 W were used to explore the effect of laser power on the joint quality. In addition, high-purity Ar gas was selected as the protection gas with a flow rate of 20 L/min to minimize the oxidation and nitrification of the welding joints, where the distance from the gas nozzle to the work piece was maintained 5 mm.

TABLE 1

Chemical composition of welded materials

Materials	Composition (wt%)								
	Cu	Ti	AL	Zr	Mo	Fe	Nb	Cr	Ni
TA15		86.94	6.5	2.29	1.80	0.08			
Inconel 718		0.849			2.95	19.1	5.19	18.83	52.53
Cu	99.9								

2.2. Characterization Methods

2.2.1. Micro-hardness Measurement

The Vickers micro-hardness of the joint was measured by a digital micro-hardness tester (HVS-1000A) with a load of 9.8 N and loading time of 15 s. Fig. 1 illustrates the testing order from the titanium alloy side to the nickel alloy side, where 6 measurement points were distributed at each base metal with an internal of 0.5 mm and 10 measurement points were distributed at the joint zone with an internal of 0.2 mm.

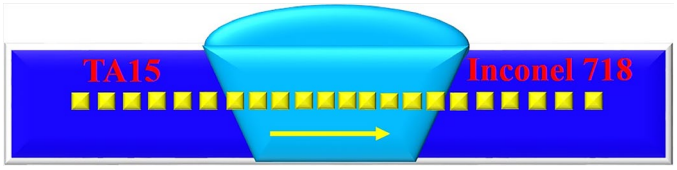

Fig. 1. Distribution of measurement points to analyze the micro-micro-hardness of joint

2.2.2. Tensile Strength Measurement

The tensile strength of the joints was measured by an electronic universal testing machine (CMT-30, Liangong testing technology, China) with a loading speed of 0.3 mm/min. The samples were prepared by a wire cutter with the size as shown in Fig. 2. The tensile strength value was determined by the average of two samples for each parameter of the laser power.

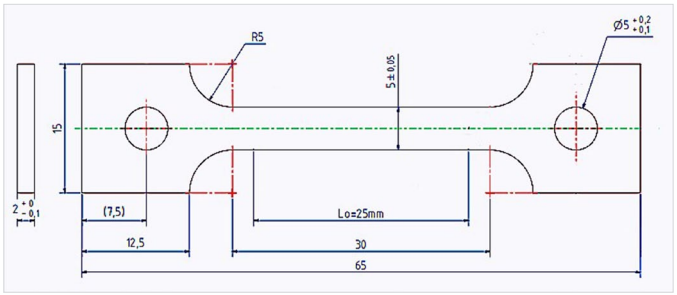

Fig. 2. Dimensional size of the sample for tensile testing

2.2.3. Microscopic Characterization

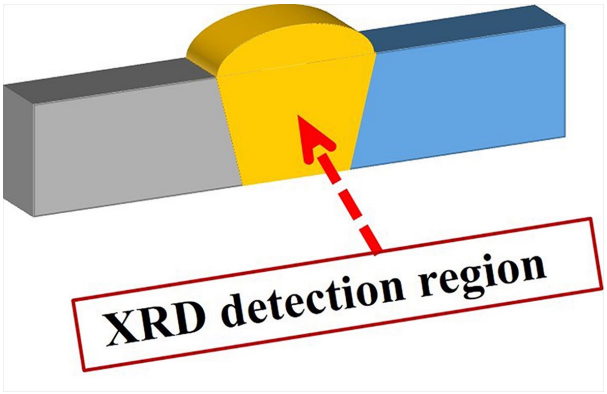

Fig. 3. Schematic diagram of XRD analysis region

After being cut by the electrospark wire-electrode cutting machine. The welding joints were sectioned using the wire cutter and then metallographically grinded and polished. The

microstructure and composition of the samples were observed by a thermal field emission scanning electron microscope (SEM) (JSM-7800F, JEOL), equipped with energy disperse spectroscopy (EDS) (Xmax80, Oxford). The phases of the joint were detected by a micro-area X-ray diffractometer (XRD) (Smart Lab) with a scanning angle of 2θ from 20° to 80°. The XRD detection area was focused on the weld zone ,as defined in Fig. 3.

3. Results and discussion

Fig. 4(a) shows the macroscopic morphology of the welding joints without Cu interlayers under 2300 W. It can be seen that a number of cracks were observed, because of Ni and Ti can form large amounts of intermetallic compounds causing the welding joints to be brittle [13,18], indicating that the dissimilar metals of the titanium alloy and the nickel alloy were not well bonded.

Fig. 4(b)-(e) show the macroscopic morphology of the welding joints with the Cu foil as interlayer under the condition of different laser powers. As shown in Fig. 4(b), it can be seen that a number of obvious pores and a rough welding surface were formed when the laser power was 2100 W. It was because that the molten pool solidified too fast when lower laser power was employed, resulting in some protective gas entering the molten pool had no enough time to escape from the molten pool. However, the formation quality of the welding joint was improved significantly with the increased laser power. When the laser power was increased to 2300 W, the quality of the welding joint was the best. With the laser power increasing further, the phenomenon of undercut was observed which could be correlated with the formation of brittle intermetallic compounds inside the welding joints.

Fig. 5 shows the micro-hardness distribution of the joints under the condition of different laser power. The T-HAZ and I-HAZ represents the heat affected zone near the TA15 base metal side and Inconel 718 base metal side, respectively. The hardness average value and standard deviation of weld zone under different laser power are shown in TABLE 2. The micro-hardness of weld zone was the higher than that of the TA15 base metal, Inconel 718 base metal and the two heat affected zones. In the T-HAZ, the hardness decreased firstly then increased with the increasing of laser power. Furthermore, the micro-hardness distribution of the joint with a laser power of 2300 W was relatively uniform with little fluctuation, while a greater fluctuation was observed for the laser power of 2100 W, and the average value was higher than the other three samples for the laser power of 2700 W. It is likely to be associated with the distribution of alloying elements in the welding joint, which was further analyzed through EDS.

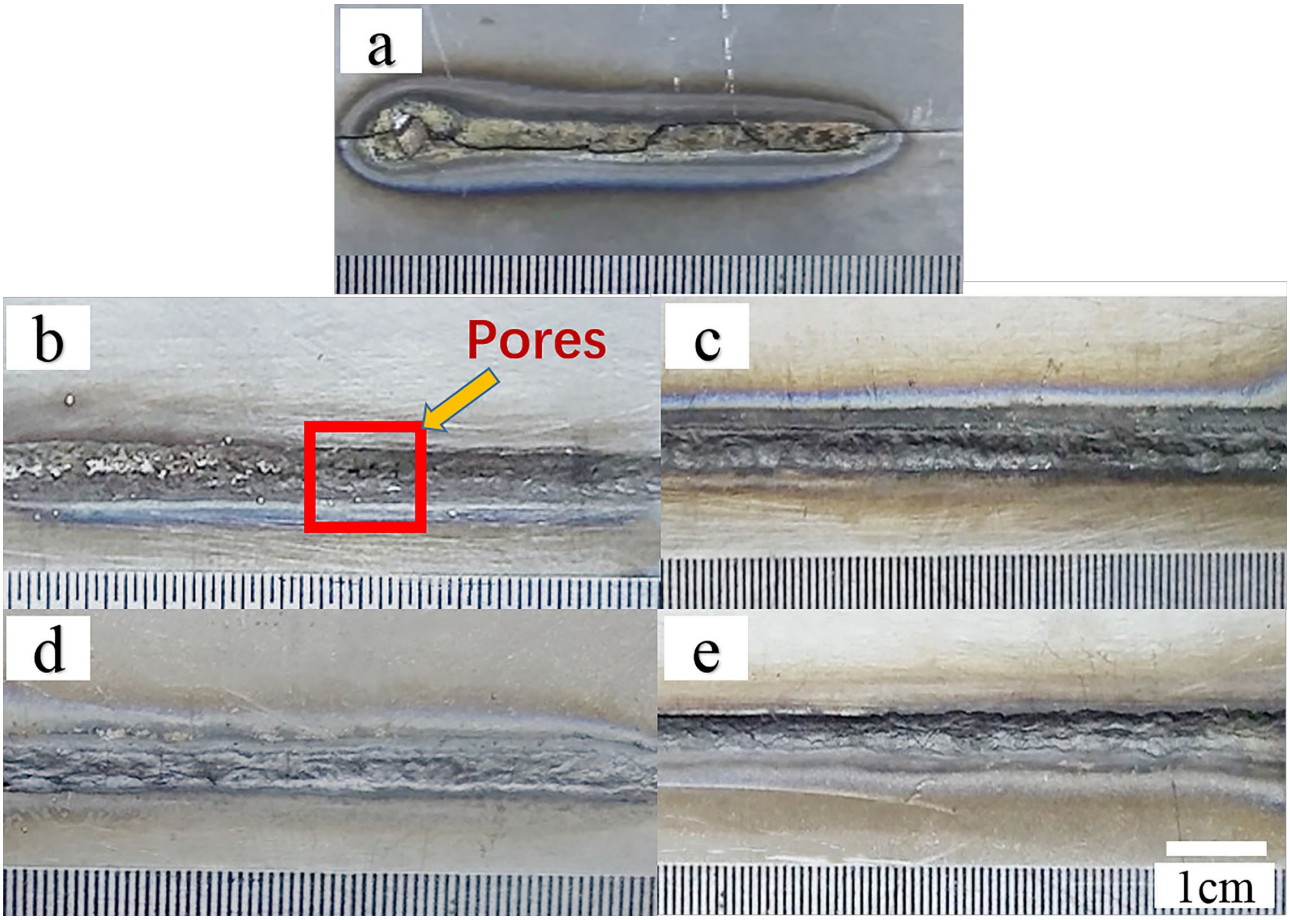

Fig. 4. The macroscopic morphology of welding joints with copper layer under different laser powers: a)without Cu interlayers under laser power of 2300 W, b) 2100 W, c) 2300 W, d) 2500 W, e) 2700 W

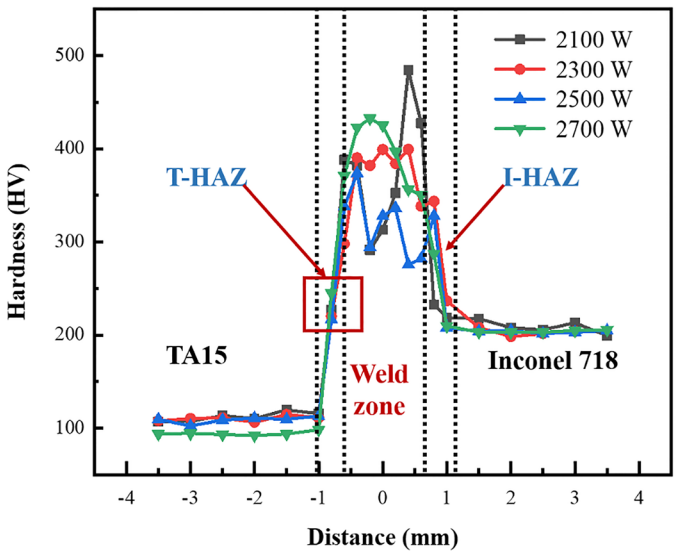

Fig. 5. The micro-hardness distribution of the joint under the condition of different laser power

TABLE 2

The hardness average value and standard deviation of weld zone under different laser power

Laser power(W)	Average Value (HV)	Standard Deviation
2100	359.03	79.74
2300	366.90	36.45
2500	319.52	33.14
2700	380.34	49.29

Fig. 6 shows the EDS line scanning results from the Inconel 718 side to the TA15 side along the welding joint. The region between the two longer dot dash lines in the figure represented the welding joint, while the zone between the two dash and dots lines on the right was the weld area near the fusion line on the TA15 side. It can be seen that elements of Ti, Cu, Ni, Cr and Mo diffused to a large distance, indicating the formation of metallurgical bonding. In the weld area near the fusion line on the TA15 side, the Ti content was higher than that of other weld area,

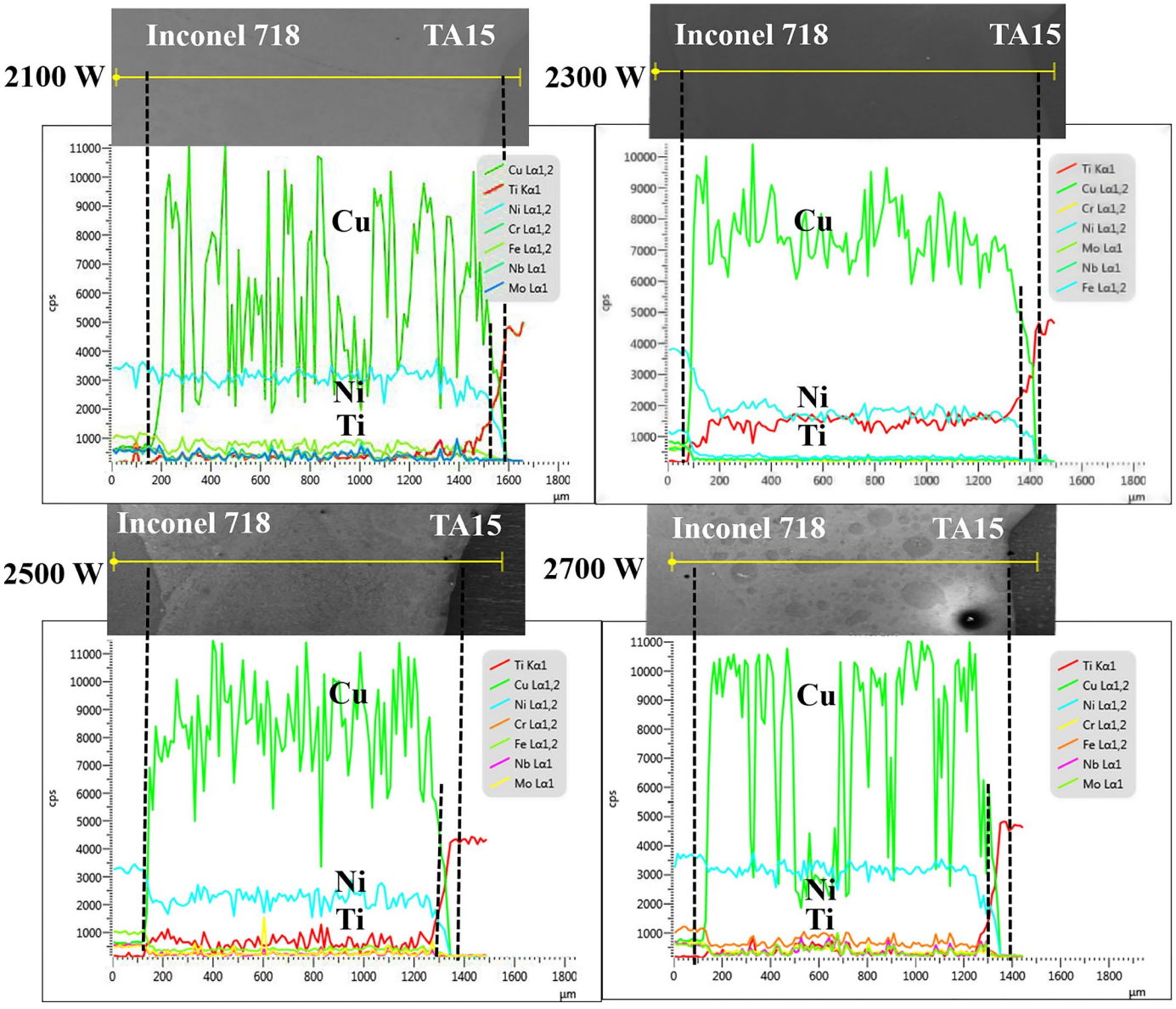

Fig. 6. EDS line scanning results of the welding joints along the cross section at different laser power of 2100 W, 2300 W, 2500 W and 2700 W

indicating that it was easier for element Ti to form intermetallic compounds with element Cu in this area. The element Cu showed the highest proportion across the welding joint, indicating that Cu was the matrix of welds. Furthermore, the fluctuation of Cu element implied that a large number of intermetallic compounds distributed inside the Cu matrix. Under the condition of 2300 W laser power, the element Cu distributed most uniformly in the welds, indicating that the intermetallic compounds distributed uniformly.

Fig. 7 shows SEM images of the joints welded at different laser power of 2100 W, 2300 W, 2500 W, 2700 W. In Fig. 7(a)-(d), the weld can be roughly divided into three parts namely the weld zone near the TA15, the weld center, and the weld zone near Inconel 718, which are represented by the number 1, 2, 3 respectively. Further microscopic division, it was observed that the microstructure of the weld area near the fusion line on the TA15 side (the area marked by the red lines) and the weld area near the fusion line on the Inconel 718 side (the area marked by the blue lines) were obviously different from other parts.

In Fig. 7(a1), the white phases marked as region A were mainly composed of the element Cu and a small amount of Ni and Ti which could dissolve into the Cu matrix. At region B, the gray phases were composed of the element Cu, Ti and Ni with an atomic ratio as 2:1.5:1, indicating that the phase was intermetallic compounds. The composition of the phases near the TA15 side was consistent even with the increase of laser power, but the microstructure became coarser generally. The microstructure of the weld area near the fusion line on the TA15 side were shown in the enlarged images of Fig. 8(T1), (T2), (T3). Fig. 9 shows the map scanning result of T1, T2, T3. The main compositions were Cu and Ti elements, indicating the microstructure of this region were intermetallic compounds composed of Cu and Ti.

In Fig. 7(a2), the brighter color phase was composed of Cu (as region E), which was the main composition of the weld, scat-

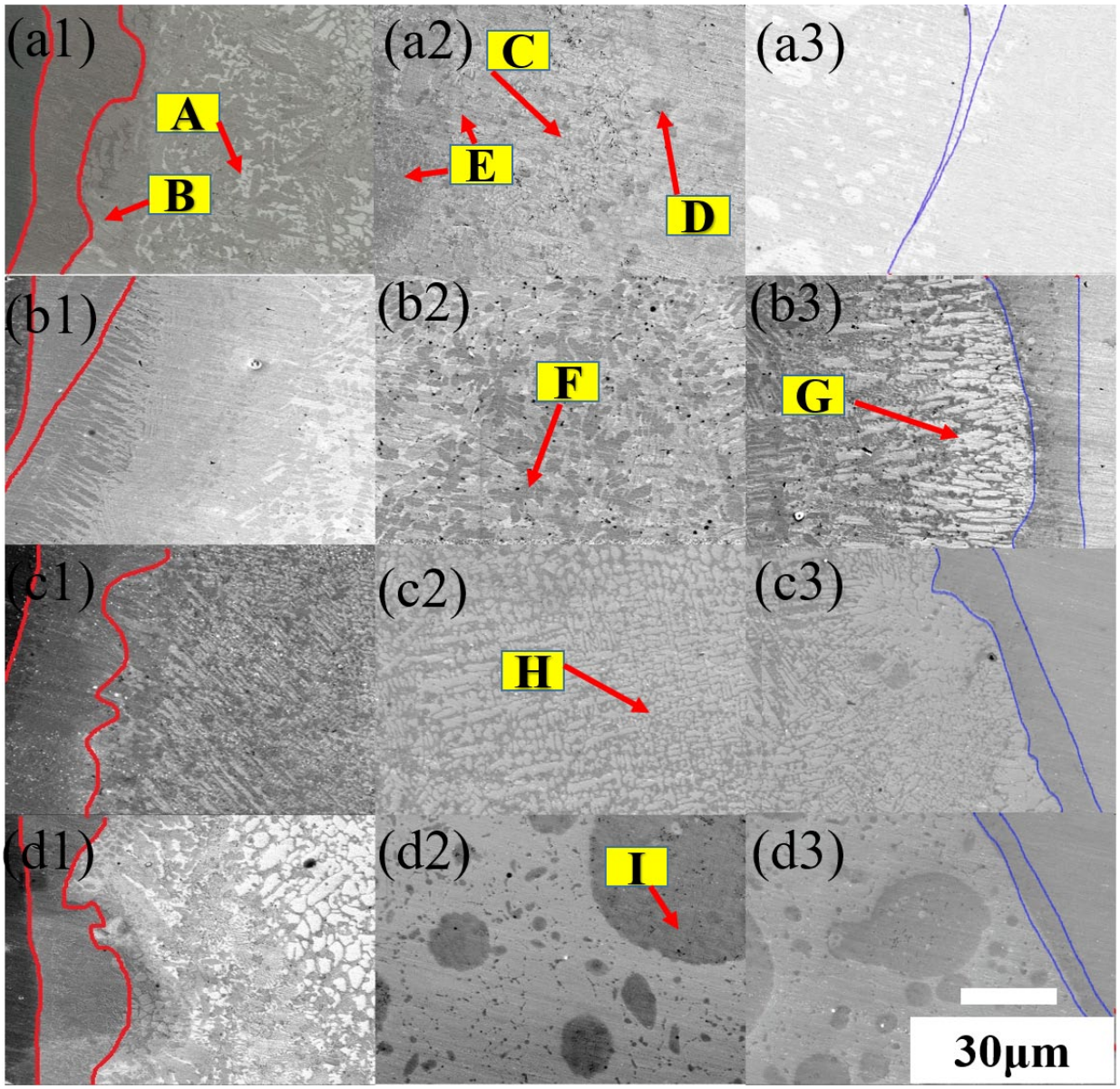

Fig. 7. SEM analysis of the joint microstructure under the condition of different laser power: (a) 2100 W, (b) 2300 W, (c) 2500 W, (d) 2700 W, and the number 1,2,3 respectively represented the weld zone near the TA15, the weld center and the weld zone near Inconel 718

tered with two petal-like phases, as shown by C and D regions, both were compounds with complex composition, as shown in Table. 3. Alloy elements such as Ni and Ti reacted in the Cu melt pool and formed new intermetallic compounds, which precipitated afterwards as the form of second-phase particles. The compositional analysis shows that the matrix of the joint was mainly composed of Cu-based solid solution, inside which a variety of intermetallic compounds scattered. It can be seen from Fig. 7(a2), (b2), (c2) that with the increase of laser power, the microstructural uniformity at the weld center was improved obviously. This is due to that the increased laser power promoted the heat input and expanded the volume of the molten pool. Accordingly, the molten pool maintained longer and the liquid metallurgical reactions proceeded sufficiently. As a result, more intermetallic compounds were formed. When the laser power is reached to 2700 W, the melting amount of the base material including Ni side increased due to the increasing of heat input, which promoted the formation of Ni-based solid solution. Therefore, as shown in the region I of Fig. 7d2), a nickel-based solid solution was generated and distributed in the weld matrix, which reduced the uniformity of microstructure. The region of the weld zone near the Inconel 718 was mainly composed of Cu-based solid solution. The brighter phases marked as region G in Fig. 7(b3) was dominated by Cu element with a percentage of 93.4% and the rest was Ni and Ti with a ratio about 1:2. Near the fusion line on Inconel 718 side, the composition of the weld zone was different from that near the TA15 sides. The enlarged SEM image of this area is shown in Fig. 8(I2). It was found that the Cu-based and Ni-based solid solutions were the main composition of the weld area near the fusion line on the Inconel 718 side. Combined with the EDS line scanning results, the Cu-based solid solution was the matrix of this region, distributing a little of intermetallic compounds. The weld area near the fusion line on the TA15 side was accumulated with various intermetallic compounds. With the increased laser power, the heat input increased, promoting the width of the accumulation layer and the content of intermetallic compounds.

TABLE 3

EDS analysis (Wt%) of the marked regions in Fig. 7

Region	Cu	Ti	Ni	Cr	Fe	Nb	Mo	Total (%)
A	85.4	3.5	8.5	0.8	1.8	—	—	100
B	47.0	28.1	22.9	0.0	2.0	—	—	100
C	—	12.1	17.6	29.1	23.1	10.5	7.6	100
D	—	10.0	13.1	48.6	23.8	3.1	1.4	100
E	53.1	34.2	12.7	—	—	—	—	100
F	78.3	21.6	0.1	—	—	—	—	100
G	93.4	4.3	2.3	—	—	—	—	100
H	93.7	3.3	3.0	—	—	—	—	100
I	24.3	9.5	36.7	12.2	12.9	3.1	1.2	100

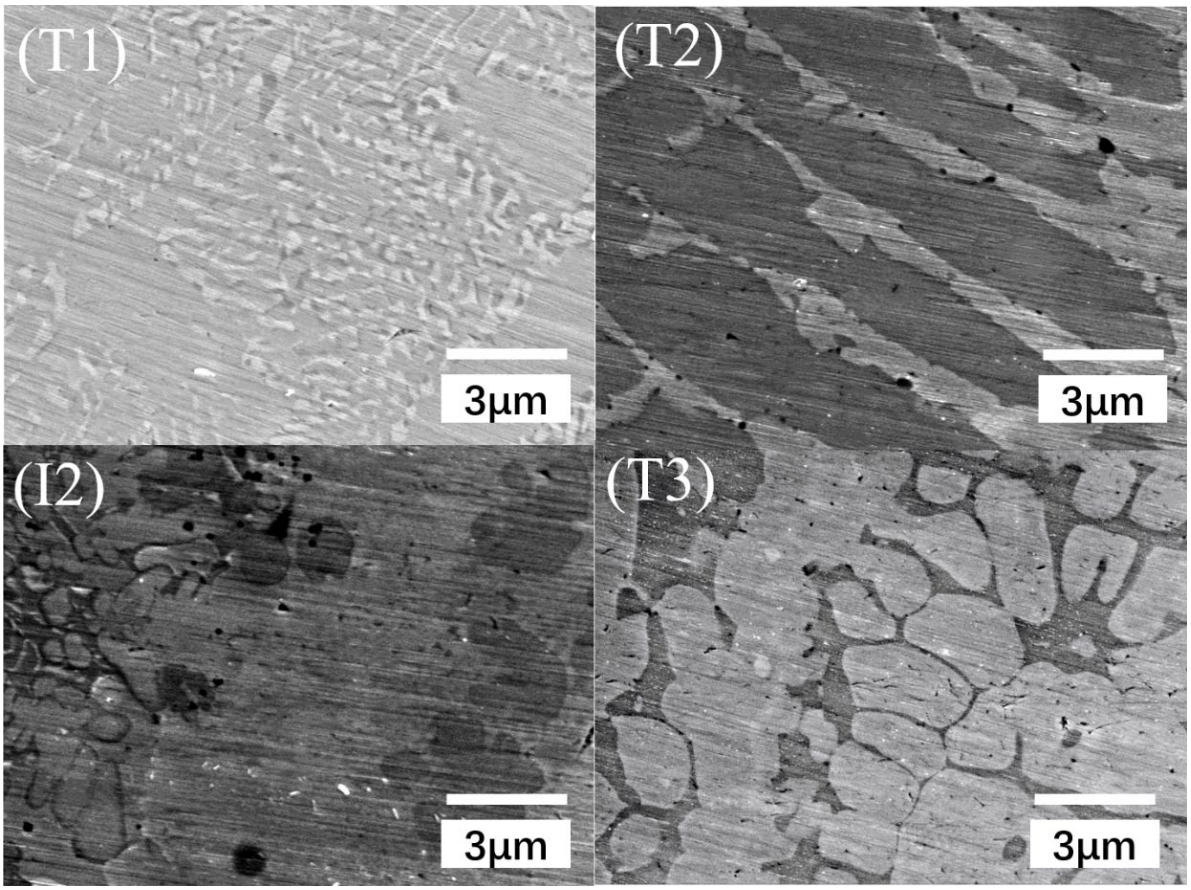

Fig. 8. The enlarged SEM image of the weld area near the fusion line: T1) the weld area near the fusion line on the TA15 side of the weld under 2100 W. T2) the weld area near the fusion line on the TA15 side of the weld under 2300 W. I2) the weld area near the fusion line on the Inconel 718 side of the weld under 2300 W. T3) the weld area near the fusion line on the TA15 side of the weld under 2700 W

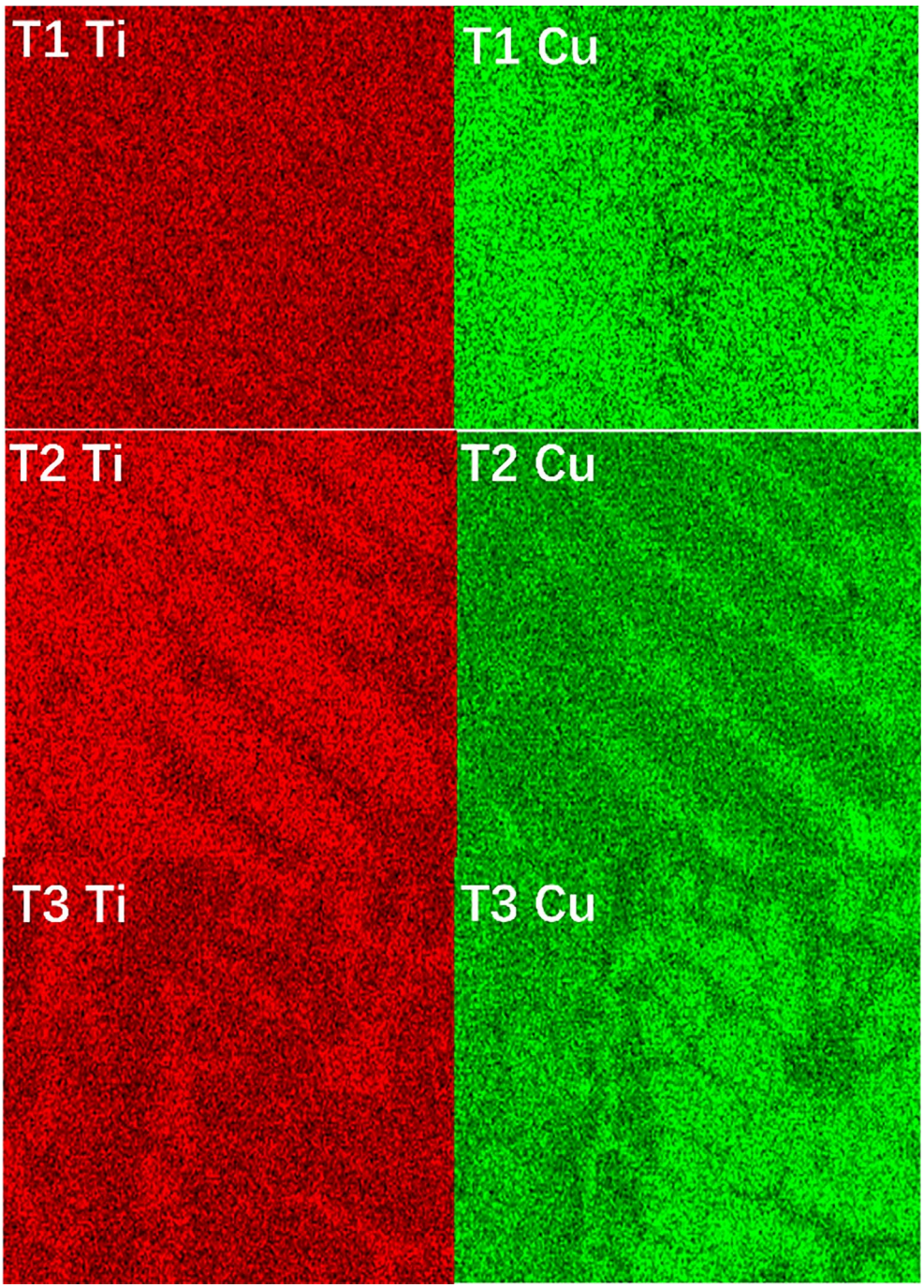

Fig. 9. The map scanning results of T1, T2, T3 in Fig. 8

In order to identify the phases of intermetallic compounds formed inside the joint, the micro-area XRD was employed and the results were shown in Fig. 10. These XRD results can prove the types of intermetallic compounds and solid solution formation mentioned in the microstructure analysis. It can be seen that the joint was consisted of Cu, and the Cu_4Ti_3 and AlNi intermetallic compounds. The diffraction peaks intensity of Cu was the highest, indicating the weld matrix was Cu, which was consistent with the results of the microstructure analysis. The intensity of diffraction peaks of Cu_4Ti_3 was more obvious than that of AlNi. According to the content Cu:Ti was 2:1.5 in Fig. 7a1) in region B, which indicated the composition of region B was Cu_4Ti_3. In addition, some weak diffraction peaks of Ti were identified. Interestingly, the elemental Ni was not found in the diffraction peaks, which was due to the easy formation of Ni solidly dissolved in Cu. This also verified the formation of nickel-based solid solution in Fig. 7d2). A comprehensive analysis of the microstructure and XRD results shows that the weld matrix was Cu, and there were Cu-based solid solutions, Ni-based solid solutions, and intermetallic compounds such as Cu_4Ti_3 in the matrix.

Fig. 11a) shows the stress-strain curve of the welding joints at different laser power. The tensile strength of the welding joints was respectively 241.7 MPa, 252.3 MPa, 241.7 MPa

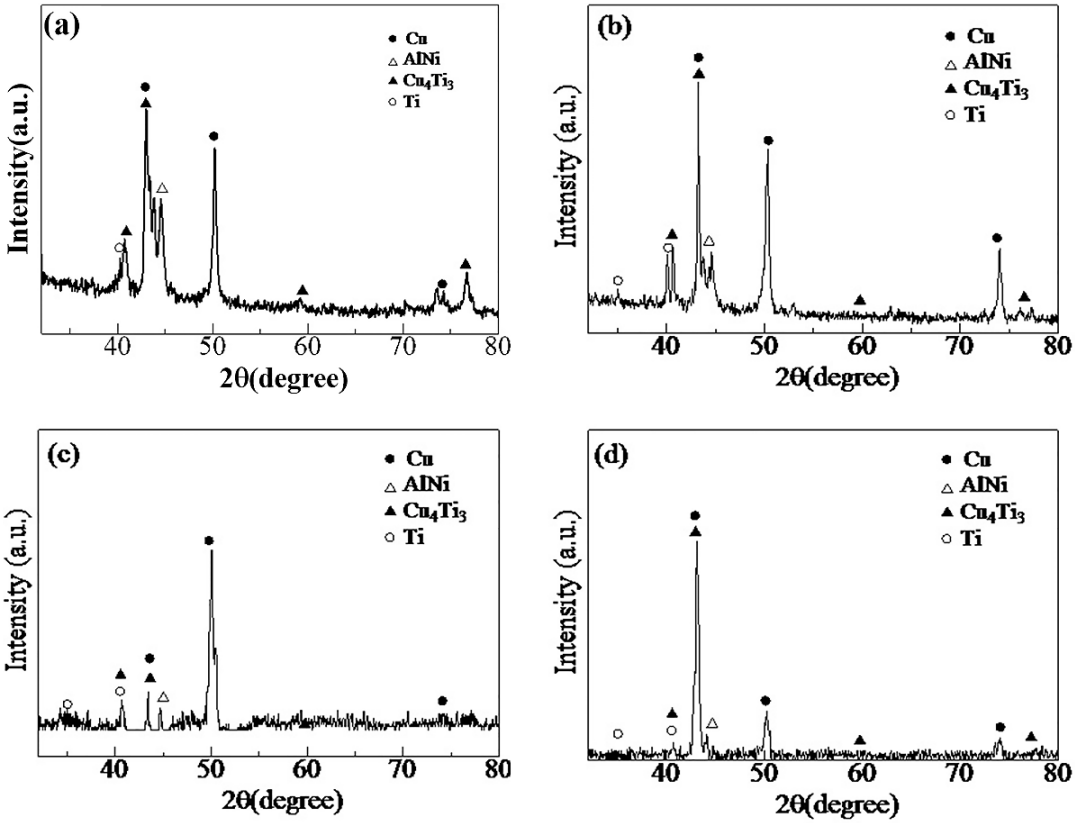

Fig. 10. The micro-area XRD pattern of welding joints center: (a) 2100 W, (b) 2300 W, (c) 2500 W, (d) 2700 W

and 229.8 MPa under conditions of 2100 W, 2300 W, 2500 W, 2700 W. The tensile strength of the welding joint with the laser power of 2300 W was the highest. No samples showed a yield stage before fracture. Considering the composition and microstructure analysis, the fluctuation of Cu content in the welding joint was the smallest and the micro-hardness was uniform when the laser power was 2300 W. This indicated that the intermetallic compounds distributed uniformly. Too large or too small laser powers could induce uneven distribution of the intermetallic compounds, decreasing the welding joint strength.

Fig. 11b) shows the macroscopic fracture morphology of the joints. The fracture position of the welding joint was close

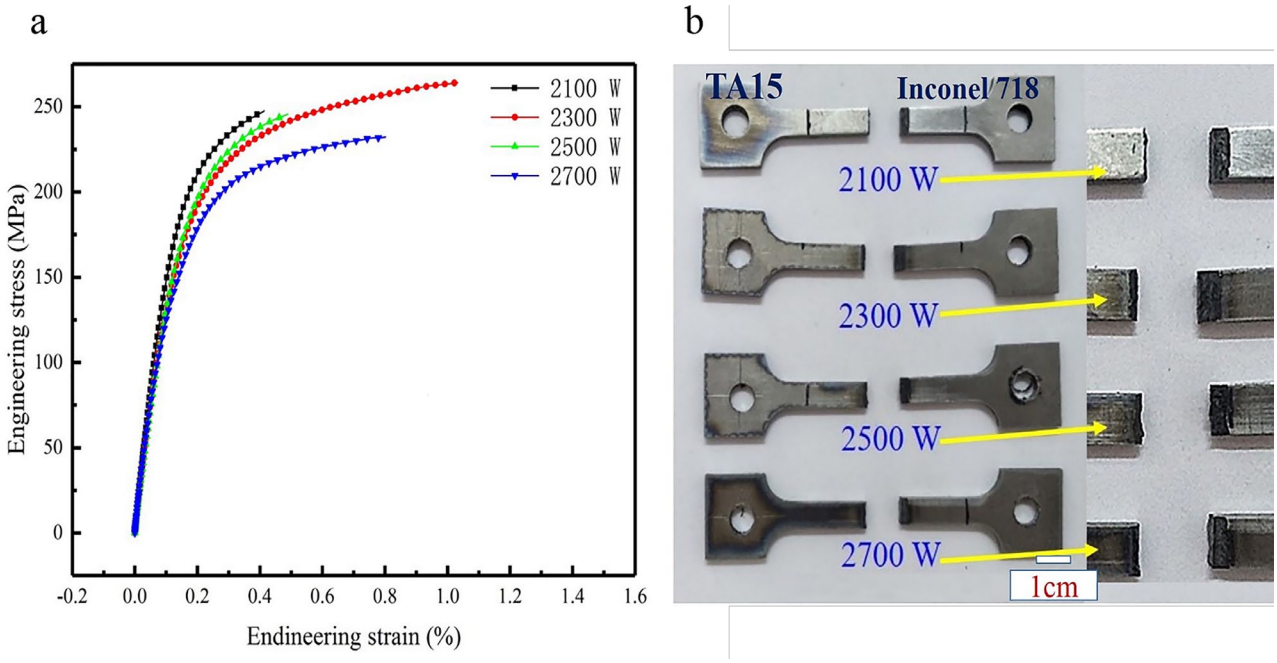

Fig. 11. a) the stress-strain curve of the welding joints tensile test, b) the macroscopic fracture morphology and fracture position

to the weld area near fusion line on the TA15 side. According the map scanning results which was shown in Fig. 9, combined with the XRD results, it was known that there were abundant Cu_4Ti_3 in the region, indicating a weak layer was formed by the accumulation of brittle compounds at this region.

Fig. 12 shows the macro and micro morphology of fractures. s1, s2, s3, s4 show macro morphology, which were cleavage type brittle fracture and can be seen the propagation of the secondary crack as marked y1, y2, y3, y4. f1, f2, f3, f4 show micromorphology, composed by many cleavage planes. An orderly cleavage step can be observed in f1, and the composition analyzed by EDS point scanning (as shown by region M) was Cu: Ti: Ni with an atomic ratio about 2:1.5:1. Combined with XRD analysis, it can be thought that the brittle Cu_4Ti_3 phase was easy to fracture in the fracture plane. f2, f3, f4 have the characteristic of river pattern, and the region N (as shown in f3) is the source of river pattern. EDS point scanning results in M and N areas are listed in TABLE 3, which indicated that the atomic ratio of Cu and Ti

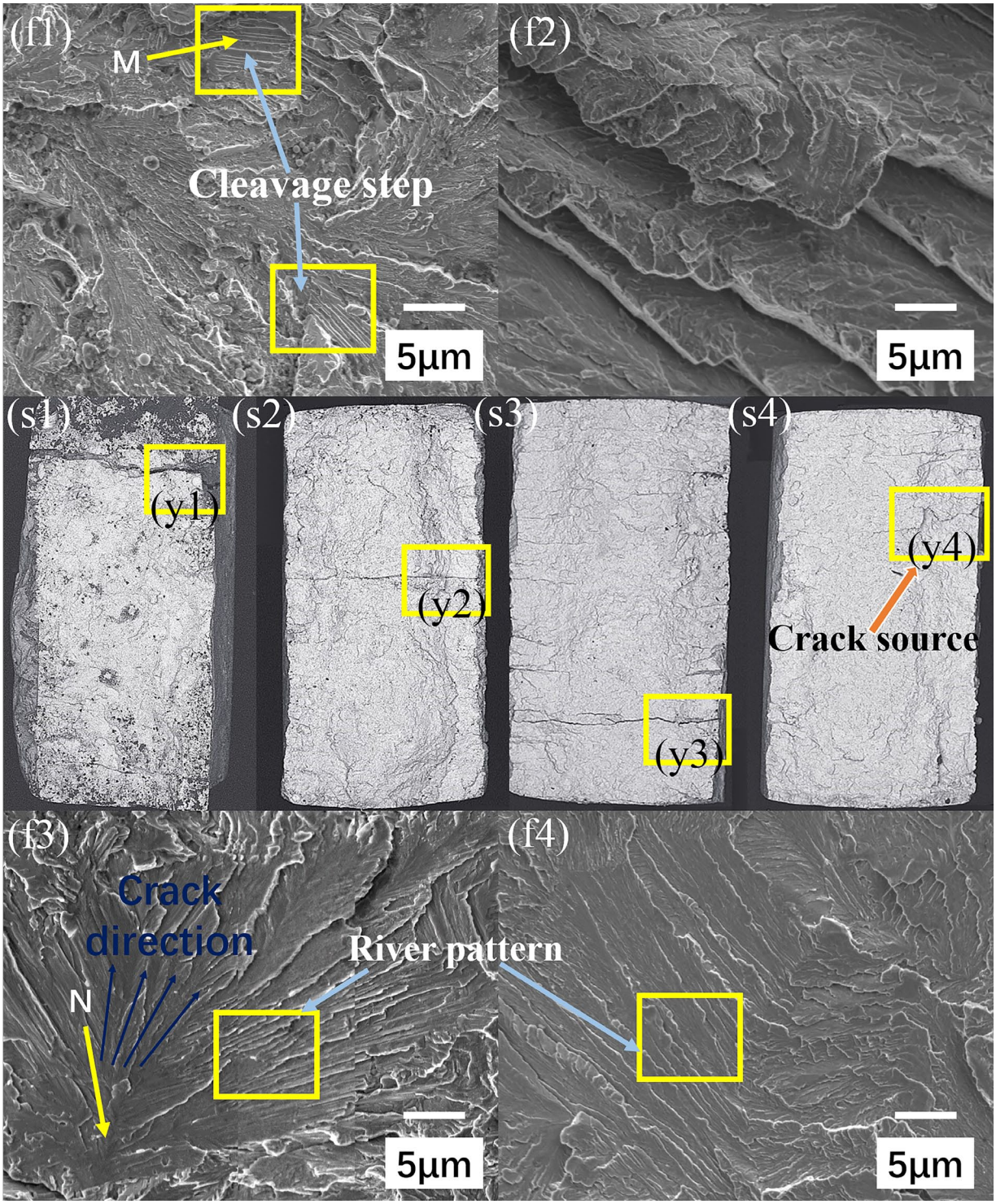

Fig. 12. s1, s2, s3, s4 and f1, f2, f3, f4 respectively was macro and micro fracture morphology of welding joints under condition of 2100 W, 2300 W, 2500 W, 2700 W

is about 2: 1.5. In conclusion, the position of fracture plane was the brittle phase enrichment zone, and the fracture mechanism was cleavage fracture.

TABLE 4

The atomic percentage of element in f1 and f3

Region	Cu (at.%)	Ti (at.%)	Ni (at.%)	Cr (at.%)	Fe (at.%)	Total (%)
M	37.2	31.7	18.8	3.2	9.1	100
N	55.4	31.9	6.7	2.0	4.1	100

4. Conclusions

This paper studied laser welding on TA15 and Inconel 718 different materials.

1. The results show that it is very difficult to obtain a well formed joint without filling layer, because of the brittle intermetallic compounds caused the welding joint fracture. Under the condition that pure Cu foil was used as the filling layer, the formation of brittle intermetallic compounds can be effectively inhibited.

2. Meanwhile, laser power had an important influence on welding joint. Under the condition of 2300 W laser power, the welding joint was formed best, the intermetallic compounds distributed uniformly, and the welding joint tensile strength was up to 252.3 MPa. Too small laser power caused poor fusion in the welding joints zone, and it was easy to form defects such as pores. Too large laser power caused more intermetallic compounds and their distribution was not uniform, which deteriorated welding joints mechanical properties.

3. The micro-area XRD results show that Cu was the main matrix of the welds, and the Cu_4Ti_3 was the main intermetallic compound, with a little of AlNi phase.

4. The fracture position after tensile test was located on the banding intermetallic compounds layer of the welding joint near the TA15. The fracture morphology had obvious characteristic of river pattern, and the fracture mechanism was cleavage fracture, belonging to brittle fracture.

Declaration of competing interest

The authors declare that they have no conflict of interest that could have appeared to influence the work reported in this paper.

Acknowledgements

This work was supported by National Natural Science Foundation of China (grant number 51975331); the fundamental research funds of Shandong University (grant number 2019HW001); key projects of laboratory construction and management in Shandong University (grant number sy20182303); and teaching reform project of Shandong University (grant number 2019Y089).

REFERENCES

[1] P. Kumar, A.N. Sinha, Weld World. **63**, 673-689 (2019).
[2] T. Yasmeen, Z. Shao, L. Zhao, P. Gao, J. Lin, J. Jiang, Int. J. Mech. Sci. **164**, 105178 (2019).
[3] Z.W. Xu, Z.W. Li, B. Chai, J.C. Yan, J. Alloy Compd. **815**, 152493 (2020).
[4] J.J Jiang, Z.H. Ren, Z.B. Ma, T. Zhang, P. Zhang, D.Z. Zhang, Z.F. Mao, Mat. Sci. Eng. A-Struct. **772**, 138742 (2020).
[5] Q.J. Sun, X. Xie, Mat. Sci. Eng. A-Struct. **724**, 493-501 (2018).
[6] K.D. Ramkumar, S.Dev, K.V. Phani Prabhakar, R. Rajendran, K.G. Mugundan, S. Narayanan, J. Mater. Process Tech. **266**, 52-62 (2019).
[7] H.C. Chen, A.J. Pinkerton, L. Li, Int. J. Adv. Manuf. Tech. **52**, 977-987 (2011).
[8] A.M. Zhao, H. Yang, X.G. Fan, P.F. Gao, R. Zuo, M. Meng, Mater. Design. **109**, 112-122 (2016).
[9] R. Ran, Y. Wang, Y.X. Zhang, F. Fang, H.S. Wang, G. Yuan, Mat. Sci. Eng. A-Struct. **793**, 139860 (2020).
[10] J.P. Oliveira, B. Panton, Z. Zeng, C.M. Andrei, Y. Zhou, R.M. Miranda, F.M. Braz, Fernandes. Acta Mater. **105**, 9-15 (2016).
[11] R.K. Devendranath, D. Sidharth, V. Saxena, A. Choudhary, N. Arivazhagan, S. Narayanan, Mater. Design. **87**, 663-674 (2015).
[12] E. Schubert, M. Klassen, I. Zerner, C. Walz, G. Sepold, J. Mater. Process Tech. **115**, 2-8 (2001).
[13] B. Onuike, A. Bandyopadhyay, Addit. Manuf. **22**, 844-851 (2018).
[14] Y.J. Fang, X.S. Jiang, D.F. Mo, D.G. Zhu, Z.P. Luo, Int. J. Adv. Manuf. Tehc. **102**, 2845-2863 (2019).
[15] C. Shang, G.J. Xu, C.Y. Wang, G. Yang, J.H. You, Mater. Lett. **252**, 342-344 (2019).
[16] M. Mehrpouya, A. Gisario, A. Brotzu, S. Natali, Opt. Laser Technol. **108**, 142-149 (2018).
[17] K-M. Hong, YC. Shin, J. Mater. Process Tech. **245**, 46-69 (2017).
[18] C. Shang, C.Y. Wang, G.J. Xu, C.F. Li, J.H. You, Vacuum. **169**, 108888 (2019).
[19] A.S. Zoeram, S.A.A.A. Mousavi, Mater. Lett. **133**, 5-8 (2014).
[20] S. Janasekaran, A. Tan, F. Yusof, M.H.A. Shukor, Metals-Basel. **6**, 134 (2016).